Replication-poison treatment in BRCA1-deficient breast cancer causes MRE11 over-resection that induces single-stranded DNA accumulation and Mitotic Catastrophe

Imene Tabet, Esin Orhan, Ermes Candiello, Lise Fenou, Carolina Velázquez, Béatrice Orsetti, Geneviéve Rodier, William Jacot, Cyril Ribeyre, Claude Sardet, et al.

Replication-Poison Treatment in *BRCA1*-Deficient Breast Cancer Causes MRE11 Over-Resection that Induces Single-Stranded DNA Accumulation and Mitotic Catastrophe

Imene Tabet[1], Esin Orhan[1], Ermes Candiello[1#], Lise Fenou[1], Carolina Velazquez[1&], Beatrice Orsetti[1], Geneviève Rodier[1], William Jacot[1,2], Cyril Ribeyre[3], Claude Sardet[1*], Charles Theillet[1*]

1. Institut de Recherche en Cancerologie de Montpellier, IRCM U1194, Montpellier University, INSERM, Institut du Cancer de Montpellier, CNRS, Montpellier, France
2. Clinical Oncology, Institut du Cancer de Montpellier, Montpellier, France
3. Institut de Génétique Humaine, CNRS UMR9002, Montpellier University, Montpellier, France

present address: University of Turin, Department of Molecular Biotechnology and Health Sciences, Turin, Italy

& present address: Department of Oncology, KU Leuven and Leuven Cancer Institute (LKI), Leuven, Belgium

* corresponding authors: Charles Theillet, IRCM INSERM U1194, ICM 34298 Montpellier cedex 5, France, Charles.theillet@inserm.fr, +33 686 92 7984

and Claude Sardet, IRCM INSERM U1194, ICM 34298 Montpellier cedex 5, France, claude.sardet@inserm.fr, +33 621 11 0021

Running title: BRCA1-deficient breast cancers are hyper-sensitive to gemcitabine

Conflict of interest:

None of the authors has a conflict of interest to disclose

Data availability

All raw data generated in this study are available from the corresponding author upon request.

Abstract

BRCA1 deficiency is observed in approximately 25% of triple-negative breast cancer (TNBC). BRCA1, a key player of homologous recombination (HR) repair, is also involved in stalled DNA replication fork protection and repair. Here, we investigated the sensitivity of BRCA1-deficient TNBC models to the frequently used replication chain terminator gemcitabine, which does not directly induce DNA breaks. A large fraction of *BRCA1*-deficient cells was sensitive to gemcitabine, in contrast to their isogenic *BRCA1*-proficient counterparts. Gemcitabine treated *BRCA1*-deficient cells accumulated massive levels of single strand DNA (ssDNA) and presented no RPA or RAD51 nuclear foci. The gemcitabine-induced accumulation of ssDNA in *BRCA1*-deficient cells was strongly diminished by targeting MRE11 with inhibitors and by siRNA attenuation. In contrast, treatment with the PARP1/2 inhibitor olaparib did not result in MRE11 dependent over-resection. Furthermore, a fraction of gemcitabine treated *BRCA1*-deficient cells that showed massive ssDNA accumulation slipped into mitosis, producing mitotic bridges and strongly stained BrdU and γH2AX micronuclei (MN). The BrdU-positive MN and DNA bridges also stained positively for cGAS. In conclusion, these data suggest that gemcitabine treatment in *BRCA1*-deficient TNBC exposes unprotected nascent DNA linked to replication fork reversal, which leads to MRE11 over-resection and ssDNA accumulation. Therefore, the observed hypersensitivity to gemcitabine indicates that it could be a beneficial addition to *BRCA1*-deficient TNBC treatment.

Significance statement

Treating BRCA1-deficient triple-negative breast cancer with gemcitabine induces massive ssDNA production due MRE11 over-resection and causes cells to slip into mitosis, produce micro-nuclei, accumulate DNA breaks, and ultimately die.

Introduction

Homologous recombination deficient (HRD) cancers, originally identified in a subset of ovarian and breast cancers with pathological *BRCA1* or *BRCA2* mutations, are characterized by an elevated genetic instability and increased sensitivity to platinum salts and PARP inhibitors (PARPi) (1). The exquisite sensitivity to genotoxic treatment of BRCA-deficient tumors has long been considered to result from faulty repair of drug-induced double-stranded DNA breaks (DSBs). However, recent data suggest that central HR players such as *BRCA1*, *BRCA2* and *RAD51* could also play important roles in the protection, repair and restart of stalled DNA replication forks (2), (3). Moreover, BRCA-deficient models exhibit diminished fork progression speed and accumulate single-stranded DNA (ssDNA) at replication forks, even in absence of exogenous stress (4), (5). Altogether, these indications support the possibility that BRCA-deficient tumors could be at particular risk of undergoing DNA replication malfunction and thus could be particularly sensitive to replication poison-based treatment. DNA replication fork stalling can have multiple causes, but in the case of anticancer drug exposure, it mainly derives from obstacles hindering fork progression or from nucleotide pool imbalance (6). Depending on the number of stalled replication forks and repair capacity, extended replication stress can result in ssDNA accumulation and affect cell viability.

Triple Negative Breast Cancer (TNBC) represent 15% of all breast cancers and its most aggressive subtype. Noticeably, TNBC comprises up to 25% of *BRCA1*-deficient tumors due to either pathological coding mutations or epigenetic silencing of the promoter (7), (8).

Given the prevalence of *BRCA1* deficiency in TNBC, we undertook to study the impact of acute replication stress induced by the replication poison gemcitabine in *BRCA1*-deficient models, by comparison with their *BRCA1*-proficients counterparts. Gemcitabine is commonly administered in cancer care and in TNBC recurrence, in combination with carboplatin (9). Our interest in gemcitabine also stemmed from the fact that, in contrast with other genotoxic drugs, it does not induce direct DNA breaks. Indeed, as an irreversible inhibitor of the large subunit of ribonucleoside-diphosphate reductase (RRM1), it impairs pyrimidine biosynthesis and produces nucleotide pool imbalance. Furthermore, being incorporated in nascent DNA, it acts as a chain terminator (10). We show here that, in comparison with their cognate *BRCA1*-proficient cells, *BRCA1*-deficient models are far more sensitive to gemcitabine, and present a large cell fraction which accumulates massive levels of single-stranded DNA (ssDNA) but no signals of the ssDNA binding protein RPA. Ultimately these cells undergo extensive DSBs and die. Our data show that the massive accumulation of ssDNA in a *BRCA1*-deficient context is associated with uncontrolled DNA resection by the MRE11 nuclease. MRE11 is an instrumental actor in DNA HR repair, and is actively recruited onto DNA DSBs by NBS1/CtIP producing

the overhangs necessary for homologous recombination (11). Interestingly, MRE11 has also been shown to be recruited by NBS1/CtIP onto stalled and reversed replication forks where it resects nascent DNA (12), (13). Furthermore, we demonstrate that a fraction of *BRCA1*-deficient cells, undergoing ssDNA accumulation, slip into mitosis, producing aberrant mitoses and micronuclei (MN) which show strong ssDNA-specific BrdU and γH2AX staining. Furthermore, these MN presented a strong cyclic GMP-AMP synthase (cGAS) signal, despite the absence of any clear activation of the IFN pathway.

Overall, our data show that *BRCA1*-deficient cancer cells are prone to undergo lethal ssDNA accumulation when treated with gemcitabine and, thus, suggest that replication chain terminators could have a favorable therapeutic impact on these tumors.

Materials and methods

Cell lines and CRISPR-Cas9 mutants.

SUM159 TNBC cells were a gift from Dr S Ethier (MUSC, Charleston, SC), MDA-MB436 (RRID:CVCL_0623), BT-549 (RRID:CVCL_1092), HCC-38 (RRID:CVCL_1267), OVCAR8 (RRID:CVCL_1629), UWB1-289PT (RRID:CVCL_B079) and the variant UWB1-289B1 (expressing a full length BRCA1 construct) (RRID:CVCL_B078), were obtained from ATCC®. Isolation and culture conditions of the CRISPR-Cas9 BRCA1-KO clone were as described (14). UWB1.289PT were cultured in 50% RPMI-1640 (Gibco™)/ 50% MEGM (MEGM Bullet Kit; CC-3150, Lonza, Basel, Switzerland) supplemented with 3% FBS, 1% Antibiotic-antimycotic (100X) (Gibco™, Fisher Scientific), HCC-38, BT-549 and OVCAR8 in RPMI-1640 supplemented with 10% FBS and 1% Antibiotic-antimycotic. All cell lines and selected clones were genetically typed by Genomics cell line authentification (Eurofins Genomics). Mycoplasma contamination was regularly assayed for all used cell lineages over the time of this project.

Immunofluorescence

Cells were grown on 12mm diameter slides cover slips in 24 well-plate for 24h, prior drug addition at predetermined IC50 concentrations. Cells and tumor sections were sequentially subjected to mild pre-extraction (PBS 0.4% Triton X100, 5min at 4°C), fixation (PBS 4% PFA) and blockage/permeabilization (PBS 3% BSA + 0.2% Triton X100, 1h at room temperature), incubated overnight at 4°C with the primary antibody (diluted in PBS 3% BSA + 0.2% Triton X100), then with the secondary antibody (diluted in PBS 3% BSA + 0.2% Triton X100, 1h at room temperature). Between each step, slides were washed 3X in PBS. Cells were counterstained with DAPI (Fisher Scientific), mounted with MWL4-88 cover slips (Citifluor, CliniSciences) and stored at 4°C. Antibodies see the Antibody section. Single-stranded DNA (ssDNA) detection experiments were performed on cells incubated with 10µM BrdU (Sigma Aldrich) for 24h prior gemcitabine treatment. BrdU was revealed with an antibody in non-denaturing conditions. In MRE11 inhibition experiments cells were incubated with 50µM Mirin (MCE- HY-117693) for 4h prior addition of gemcitabine and maintained alongside gemcitabine for 24h

Immunofluorescence images were acquired on a Zeiss microscope (RRID:SCR_024706) equipped with a 63X-immersion oil lens and Zeiss Blue software (RRID:SCR_013672). Cells with ≥5 to 10 nuclear foci depending on the target protein were scored using CellProfiler (RRID:SCR_007358). At least three biological replicates (vehicle-, gemcitabine- and olaparib-treated) were quantified.

For tumor tissues, 6µm cryosections were prepared from OCT embedded deep frozen tissue and mounted on Fisherbrand™ Superfrost™ Plus Microscope Slides (Fisher Scientific) and stored at -80°C

until used. Tumor cryosections were immersed in 70% ethanol containing 0.1% SBB (Sigma Aldrich) for 20min at RT to reduce autofluorescence and washed 3X 5min in PBS with 0.02% Tween 20. Subsequent immunostaining steps were identical to those applied on cell lines.

Cell cycle determination and replication stress quantification by flow cytometry

$7x10^5$ cells were grown for 24h and subjected to a 30min pulse with 10µM EdU Click-it (ThermoFisher Scientific) prior 100nM gemcitabine-treatment for 24h. After drug removal fresh medium was added and cell aliquots were collected at time points 0h, 8h, 24h, 48h. Cells were trypsinized and spun at 1200 rpm for 5min. Cell pellets were resuspended in the pre-extraction solution (PBS + 0.4% Triton X100) for 5min, pelleted, fixed with 4%PFA in PBS for 30min at RT and permeabilized in PBS + 1% BSA + 1X saponin for 20min at RT. Cells were sequentially incubated for with the primary and the secondary antibodies diluted in PBS + 1%BSA + 1X saponin for 60 and 30min at RT. Between primary and secondary antibody incubation cells were washed in PBS+1%BSA. After secondary antibody incubation cells were resuspended in PBS + 1%BSA + 1µg/ml DAPI for DNA counterstaining. FACS analysis was performed on a Gallios Flow Cytometer (RRID:SCR_019639). Debris and doublets were excluded. Settings were identical in each channel and 10 000 cells were analyzed per aliquot. The quantification of the sub-G1 fraction settings partially excluded debris and doublets. Quantification of apoptosis was done on cell pellets rinsed once in cold PBS and a second time in cold BBA buffer (10mM HEPES pH7.4, 110mM NaCl, 2.5mM CaCl2). Cells were resuspended in 50µl BBA buffer + 1µl AnnexinV (Sigma Aldrich) and 0.02µg Propidium Iodide (PI) and incubated at RT for 30min. Prior cell analysis 200 µl PBS were added. Mitotic-slippage was evaluated on cells synchronized in G1 with 100nM of the CDK4/6 inhibitor palbociclib for 24h. Cells were washed and released for 24h, before adding 1µM gemcitabine for 3h. FACS gating and cell cycle synchronization strategies can be seen at DOI: 10.6084/m9.figshare.28003310.

Cell viability test

Experiments were performed in 96 well flat bottom plates (Starstedt) with 1500 cells seeded in each well. After 24h 10µl serial drug dilutions were added in row of 8 wells. This was repeated in triplicates. Cells were exposed to the drug for 24h (equivalent to a complete doubling time in these cells), gently pelleted and resuspended in fresh medium and left for approximately 2 cell cycle periods (48-56h), before addition of 10µl CCK8 (Cell Counting Kit-8, Tebubio). Multi-well plates were incubated for 4h at 37°C, solutions in the wells gently homogenized and 450nM OD were measured on a FLUOstar omega, BMG Labtech (RRID:SCR_025024). Cell viability (%) = [(As-Ab) / (Ac-Ab)] × 100; As represents the absorbance of the experimental well, Ab the absorbance of a control well

containing medium and CCK8, Ac the absorbance of a control well containing cells, medium and CCK8.

Protein extraction and Western blotting

Protein extracts were prepared by lysing either tumor tissue or cell line pellets on ice for 30min in 50mM Tris-HCl pH7.4, NaCl 100mM, NaF 50mM, β-glycerophosphate 40mM, EDTA 5mM, Triton X100 1%, Aprotinin 10mg/ml, PMSF 100mM, Leupeptin 1mM, Pepstatin 1mM, followed by a short centrifugation to pellet debris. Protein concentrations were measured using the BCA kit (Fisher Scientific) SDS-PAGE gel electrophoresis was performed on 60µg protein samples subsequently transferred onto 0.22 µm nitrocellulose membranes (Amersham) and incubated overnight at 4°C with the primary antibody, after blocking for 1h in 10 % non-fat milk in TBST buffer (20mM Tris-HCl pH7.4, 150mM NaCl, 0.05% Tween20). Antibodies used are listed in a separate section. Membranes were then washed and incubated with the appropriate secondary antibody in 5% non-fat dry milk in PBST for 2h at RT and revealed in Chemiluminescent HRP Substrate (Sigma Aldrich).

Genomic DNA double-stranded DNA break determination by Pulse Field Gel Electrophoresis (PFGE)

Pellets of $1x10^6$ treated cells were incorporated in 1% agarose at 50°C and cast into molds (Biorad) avoiding air bubbles. Samples in agarose plugs were incubated in lysis buffer (100mM EDTA pH8, 0.2% sodium lauryl sarcosine, 1mg/ml proteinase K) for 24h at 37°C, rinsed 3 times in wash buffer (20mM Tris, 50mM EDTA pH9) and positioned in the wells of a 1% agarose gel in 0.25X TBE. The gel was then run for 24h using pulsed electric field. DNA was labeled using Syber Green and revealed by UV. Fragmented DNA was quantified using the Image lab 6.0.1 software (RRID:SCR_014210), and normalized relative to the non-fragmented DNA intensity.

PDX models and in vivo treatment

TNBC PDX models establishment was as described (15). The study was reviewed and approved by the ethics committees for animal experimentations of the University of Montpellier (CEEA-LR-12028) and received the approval number 25612. PDX models were established from fresh tumor fragments obtained from the Pathology Department at the Comprehensive Cancer Center of Montpellier (ICM). Patients whose tumor was used to generate PDX signed informed consent forms.

Approximately 50 mm^3 PDX fragments were grafted subcutaneously into the flank of 3-4week old Swiss-nude female mice (Charles Rivers, Saint-Germain-sur-l'Arbresle, France). The present study comprised two experimental arms; vehicle and gemcitabine (Lilly, Fegersheim, France) comprising 8 mice per arm. When median tumor volume reached 100-150mm3, mice were randomly distributed in the two arms and treatment was started. Gemcitabine was injected intra-peritoneally (IP)

twice/week for 4 weeks at 50 mg/kg. At treatment end, mice were euthanized, tumor samples collected for further histological analyses.

Antibodies

immunofluorescence/FACS : Mouse anti-BrdU 1/200 (BD Biosciences Cat# 347580, RRID:AB_10015219), mouse anti-BRCA1 1/300, (Santa Cruz Biotechnology Cat# sc-6954, RRID:AB_626761), rabbit anti-BRCA2 1/500, (Bethyl Cat# A303-434A, RRID:AB_10952240), rabbit anti-phospho histone 3 1/50, (Cell Signaling Technology Cat# 9701, RRID:AB_331535), rabbit anti-53BP1 1/2000, (Novus Cat# NB100-34, RRId:AB_3665239), rabbit anti-MRE11 1/3000 (Novus Cat# NB100-142, RRID:AB_10077796), rabbit anti-RAD51 1/300, (Millipore Cat# PC130, RRID:AB_2238184), mouse anti-RPA32 1/200, (Abcam Cat# ab2175, RRID:AB_302873), rabbit anti-SMARCAL1 1/500 (Santa Cruz Biotechnology Cat# sc-166209, RRID:AB_2191695), rabbit anti-γH2AX 1/1000 (Cell Signaling Technology Cat# 9718, RRID:AB_2118009). Secondary antibodies; anti-rabbit alexa fluor 555 1/100, (Abcam Cat# ab150075, RRID:AB_2752244, anti-mouse alexa fluor 488 1/1000, (Abcam Cat# ab150113, RRID:AB_2576208). Western blotting: rabbit anti-BRCA1 1/500, (Cell Signaling Technology Cat# 9010, RRID:AB_2228244), rabbit anti-BRCA2 1/500, (Bethyl Cat# A303-434A, RRID:AB_10952240), rabbit anti-RAD51 1/1000, (Cell Signaling Technology Cat# 8875, RRID:AB_2721109) Secondary antibodies; anti-rabbit HRP 1/10000 (Cell Signaling Technology Cat# 7074, RRID:AB_2099233), anti-mouse HRP 1/10000, (Cell Signaling Technology Cat# 7076, RRID:AB_330924).

Ethics and data availability

TNBC PDX models were established from fresh tumor fragments obtained from the Pathology Department after informed consent of the patients and approval by the institutional review board of the Comprehensive Cancer Center of Montpellier (ICM) as described (15). The *in vivo* study was reviewed and approved by the ethics committees for animal experimentations of the University of Montpellier (CEEA-LR-12028. Data produced as part of this study are available upon reasonable request to the corresponding authors.

Results

BRCA1-deficient cell models exhibit increased sensitivity to gemcitabine

We determined the sensitivity to gemcitabine of 5 cell lines (4 TNBC and 1 ovarian cancer) with different *BRCA1* statuses; *BRCA1* wild type (BT-549 and SUM-159B1), *BRCA1*-mutated (MDA-MB-436) and full (OVCAR8) or partial (HCC-38) *BRCA1*-promoter hypermethylation (16, 17). In addition, we engineered by CRISPR-Cas9 a *BRCA1*-KO clone (SUM-159B1KO) from the SUM-159B1WT cell line (14). Noticeably, *BRCA1*-deficient cell lines MDA-MB-436, OVCAR8 and SUM-159B1KO showed distinctly lower IC50 to gemcitabine, compared with the *BRCA1*-proficient BT-549 and SUM-159B1WT and the partially *BRCA1*-hypermethylated TNBC cell line HCC-38 (Figure 1A). Western blotting analysis revealed that, while BRCA1 protein was clearly expressed in SUM-159, BT-549 and HCC-38, it was not detectable in the *BRCA1*-deficient SUM-159B1KO, MDA-MB-436 and OVCAR8 cell lines (Supplementary Fig 1A). We also verified the protein expression levels of the important HR co-factors of BRCA1, BRCA2 and RAD51. Noticeably, all cell lines expressed similar BRCA2 and RAD51 levels. These data, thus, suggested that the higher sensitivity to gemcitabine could be linked to the absence of BRCA1 protein expression. Next, we focused our study on the isogenic SUM-159B1WT and SUM-159B1KO cell line pair and noted that the mortality induced by 100nM gemcitabine in SUM-159B1KO cells was five-fold that in SUM-159B1WT (Figure 1B).

Thereafter, we applied a gemcitabine treatment protocol similar to that used for IC50 determination (14), *i.e.* 24h drug exposure followed by drug removal and analysis at different time points (Figure 1C). Cell cycle analysis of SUM-159B1WT and SUM-159B1KO cells treated with 100nM gemcitabine (IC50 of SUM-159B1WT) revealed that SUM-159B1WT cells reentered the cell cycle 48h after removing the drug, while SUM-159B1KO further continued to accumulate in S and G2/M cell cycle phases (Supplementary Fig 1B-C).

These data indicated that BRCA1-deficient cells treated with the replication poison gemcitabine undergo severe mortality combined with a strong G2/M blockage.

BRCA1-deficient cells exhibit strongly-reduced RAD51 and BRCA2 foci formation upon gemcitabine treatment

While RAD51 and BRCA2, play important roles in HR DSB repair, their involvement in the protection and repair of stalled replication forks has also been demonstrated (18). We, therefore, performed an immunofluorescence time-course monitoring of nuclear RAD51 and BRCA2 foci formation levels, in conjunction with that of BRCA1 in gemcitabine-treated SUM-159B1KO and SUM-159B1WT. Furthermore, we scored foci numbers of 53BP1, a protein that strongly binds to DSB and is actively antagonized by BRCA1 (19). There is, thus, an inverted balance between BRCA1 and 53BP1 on DSBs,

which we wanted to assess in situations of replication stress. Interestingly, whereas SUM-159B1WT treated with 100nM gemcitabine showed a strong increase in BRCA1, BRCA2 and RAD51 foci formation, peaking at 8h and slowly receding after 24h, BRCA1, BRCA2 and RAD51 foci formation was strongly impaired in SUM-159B1KO (Figure 1D-E). By contrast, 53BP1 foci numbers increased significantly in SUM-159B1KO (Figure 1F-G). We made very similar observations in the *BRCA1* mutated UWB1.289PT ovarian carcinoma cell line, in comparison with its UWB1.289B1 variant ectopically expressing a WT *BRCA1* construct and observed impaired BRCA2 and RAD51 associated with increased 53BP1 foci formation in parental UWB1.289 cells (Supplementary Fig 1D-E). These results showed that BRCA1-deficient models present impaired BRCA1/2 and RAD51 nuclear recruitment associated to a strong recruitment of 53BP1 upon gemcitabine treatment.

Gemcitabine-treated BRCA1-deficient models undergo persistent replicative stress

Cell populations subjected to replication stress exhibit increased γH2AX-positive and RPA-positive cell numbers, but in case of acute replication stress γH2AX-positive cells outnumber RPA-positive cells (20). We performed a FACS time course analysis of γH2AX-positive and RPA-positive cells in gemcitabine-treated SUM-159B1WT and SUM-159B1KO. We noted a temporary imbalance of γH2AX-positive and RPA-positive cell numbers at 0h and 8h in SUM-159B1WT (Figure 2A), whereas SUM-159B1KO exhibited a strong and persistent γH2AX/RPA imbalance (Figure 2B). The excess of γH2AX-positive relative to RPA-positive cells in gemcitabine-treated SUM-159B1KO in comparison with SUM-159B1WT was also detectable by immunofluorescence (Figure 2C-F). While the number of γH2AX-positive cells remained stable between 24h and 48h, the fraction of RPA-positive cells steadily decreased at 24h and 48h in SUM-159B1KO (Figure 2F). In identical conditions, SUM-159B1WT showed no imbalance between γH2AX-positive and RPA-positive cells and decreasing numbers of γH2AX-positive and/or RPA-positive cells at 48h (Figure 2C-D). Interestingly, FACS profiles revealed that cells showing γH2AX/RPA imbalance were distributed from early S to G2/M cell cycle phases (Supplementary Fig 2A-B). We made similar observations in UWB1.289PT and UWB1.289B1 cells. The parental *BRCA1*-deficient UWB1.289PT cells showed a strong imbalance between γH2AX-positive and RPA-positive cells, whereas its isogenic BRCA1-proficient variant UWB1.289B1 did not (Supplementary Fig 2C-F). These data therefore support that *BRCA1*-deficiency is associated with an acute and persistent replication stress upon gemcitabine treatment.

BRCA1-deficient cells accumulate large quantities of ssDNA and pan-nuclear γH2AX-staining in absence of RPA signal.

As revealed by BrdU immunostaining under non-denaturing condition, gemcitabine-treated cells accumulated ssDNA, with some cells showing intense BrdU staining (Figure 3A). The number of cells showing this intense BrdU staining was distinctly higher in SUM-159B1KO than in SUM-159B1WT

(Figure 3B). Strikingly, most of these cells presented no signal for the ssDNA binding protein RPA (Figure 3C, D). In SUM-159B1KO, BrdU-positive/RPA-negative cell numbers gradually increased over time in SUM-159B1KO, reaching up to 65% of the cell population at 48h (Figure 3D). By contrast, within the same time frame, BrdU-positive/RPA-negative cells did not exceed 20% in SUM-159B1WT (Figure 3B). Noticeably, cells with intense BrdU-staining were also characterized by a strong pan-nuclear γH2AX-staining (Figure 3E-G, Supplementary Fig 3A). Furthermore, most cells with pan-nuclear γH2AX-staining presented no RPA foci (Figure 4A-B). Strikingly, the BrdU (ssDNA)/ pan-nuclear γH2AX-positive cells were mainly observed in SUM-159B1KO and other *BRCA1*-deficient cell models, where their numbers strongly increased over time, reaching up to 70% of the BrdU-positive cells 48h after drug removal (Figure 3F-G, Supplementary Fig 3B-D). The absence of RPA signals in a subset of SUM-159B1KO cells suggested the possibility of a reduction of RPA protein levels in these cells. However, SUM-159B1WT and SUM-159B1KO showed similar levels of RPA32 protein by western blot (Figure 4C). Notably, the analysis of protein extracts prepared from subcellular fractionation revealed that, whereas cytoplasmic RPA32 levels were equivalent, those recruited to the chromatin were distinctly lower in gemcitabine-treated SUM-159B1KO compared with SUM-159B1WT (Figure 4D). These data, thus, suggest a defect in chromatin recruitment of RPA32 in a BRCA1-defective context. We also sought to determine RAD51 and 53BP1 staining patterns in pan-nuclear γH2AX staining cells. Remarkably, a large majority of SUM-159B1KO cells with pan-nuclear γH2AX staining showed no RAD51 foci (pan-nuclear γH2AX-positive/RAD51-negative). Contrastingly, up to 80% of pan-nuclear γH2AX-positive SUM-159B1KO cells showed elevated numbers of 53BP1 foci as compared to SUM-159B1WT where 53BP1 positive cell numbers did not exceed 30% (Figure 4E-H).

Our results thus indicate that, in BRCA1-deficient models, gemcitabine treatment results in a gradual and persistent increase in ssDNA accumulation in absence of RPA and/or RAD51 binding.

MRE11 attenuation or inhibition strongly reduced ssDNA accumulation and DSB levels in gemcitabine-treated SUM-159B1KO cells

The absence of RPA, RAD51 and reduced BRCA2 levels in gemcitabine-treated SUM-159B1KO cells constituted a context of poor fork protection favorable to uncontrolled MRE11 DNA resection (3),(18),(21). Consistent with this scenario, treatment of SUM-159B1KO cells with 100nM gemcitabine + 50μM of the MRE11-inhibitor mirin resulted in a considerable reduction of BrdU-positive and γH2AX-positive cell numbers. By contrast, mirin addition induced only marginal changes in SUM-159B1WT (Figure 5A-F). Interestingly, we also observed a strong reduction in BrdU-positive and γH2AX-positive cell numbers when the MRE11 endonuclease inhibitor PFM39 or siRNA attenuation of *MRE11* expression were combined with gemcitabine (Supplementary Fig 4A-M).

Altogether, these data support the notion that MRE11 plays a fundamental role in the ssDNA accumulation in gemcitabine-treated BRCA1-deficient cells.

Furthermore, as unresolved replication fork stalling and breakdown can result in double-stranded DNA breaks (DSBs), we employed pulse field gel electrophoresis (PFGE) to determine DSB levels in gemcitabine-treated SUM-159B1WT and SUM-159B1KO. In identical conditions, gemcitabine-treated SUM-159B1KO accumulated at least two times more DSBs than SUM-159B1WT. Furthermore, while its effect was not as pervasive in SUM-159WT (Figure 5G, Supplementary Fig 5A), mirin addition strongly reduced DSB levels in SUM-159B1KO, in line with the impact of MRE11 inhibition on ssDNA accumulation (Figure 5B, 5E). However, it has been suggested that, in BRCA2-defective models treated with the PARP1/2 inhibitor olaparib, DNA breaks might be the result of apoptotic DNA fragmentation, rather than of replication fork breakdown (22). Hence, we verified the impact of the pan-caspase inhibitor ZVAD-FMK (50µM) on gemcitabine-treated SUM-159B1KO and SUM-159B1WT, but observed no reduction in DSB levels, despite a strong reduction in apoptotic cell numbers (Figure 5H, Supplementary Fig 5B-E). Hence, our data indicated that uncontrolled MRE11 resection plays a major role in the accumulation of ssDNA in gemcitabine-treated BRCA1-deficient models and is associated with a strong increase in DSBs.

While MRE11 resection plays a leading role in gemcitabine-induced ssDNA accumulation, this is not the case in olaparib-treated cells.

We further questioned whether MRE11 resection would also be observed in *BRCA1*-deficient cells upon PARP1/2 inhibitor olaparib treatment. Thus, we tested the impact of MRE11 resection on ssDNA accumulation in cells treated with 100µM (IC50 measured in SUM-159B1WT) olaparib +/- 50µM mirin for 24h. Remarkably, neither SUM-159B1WT nor SUM-159B1KO showed any significant reduction of either BrdU (ssDNA) or γH2AX levels upon mirin addition. These data indicated that MRE11 resection does not play a major part in olaparib-induced replication stress (Figure 5I-5N). The prevalent role of MRE11-dependent resection in gemcitabine–treated SUM-159B1KO ssDNA accumulation led to speculate on the potential involvement of replication fork reversal in this process. In response to acute replication blockage, fork reversal puts replication forks on hold in the perspective of repair, but it also produces nascent DNA overhangs, which are vulnerable to nucleolytic attack (23). Due to the absence or limited availability of RAD51, these structures are particularly vulnerable to MRE11 resection in *BRCA*-deficient cells (12), (13),(18),(24),(25). Significantly, we noted that SMARCAL1, which is a major actor involved in fork reversal, was strongly recruited at the chromatin in gemcitabine-treated cells (Supplementary Fig 6A), and showed intense accumulation in SUM-159B1KO nuclei (Supplementary Fig 6B-E). Interestingly, nuclear recruitment of SMARCAL1 was not as marked upon olaparib treatment (Supplementary Fig 6A-E). Hence, these

results suggest that while gemcitabine treatment induces MRE11-dependent hyper-resection, possibly associated with enhanced fork reversal, this does not occur upon olaparib treatment.

SUM-159B1KO cells undergoing acute replication stress slip into mitosis resulting in mitotic catastrophe.

*W*e previously determined that gemcitabine-treated BRCA1-deficient cells tended to accumulate in G2/M (Supplementary Fig 1C) and formed micronuclei (MN), suggesting possible mitotic catastrophes. Hence, we considered the possibility that gemcitabine-treated SUM-159B1KO cells may have a tendency to slip into mitosis. To ascertain this, we synchronized the cells at the end of G1 by exposing them to 100nM of the CDK4/6 inhibitor palbociclib for 24h. Cells reached S phase synchronously 8h after palbociclib removal, time at which we added 1µM gemcitabine for 3h (Supplementary Fig 7A). After removing gemcitabine, FACS monitoring revealed that, while SUM-159B1WT resumed the cell cycle between 72 and 96h, SUM-159B1KO accumulated in M phase at identical time points (Supplementary Fig 7B, 7C). Interestingly, the cell cycle profile of gemcitabine-treated SUM-159B1KO was similar to that of cells treated with a combination of 50nM gemcitabine + 50nM of the CHK1 inhibitor PF-0477736 (Supplementary Fig 7D), suggesting that SUM-159B1KO presented a defective G2 to M checkpoint (26). Unscheduled progression into mitosis was in line with the large fraction of aberrant mitoses (multipolar divisions, mitotic bridges or MN), representing up to 70% of the mitotic figures observed in gemcitabine-treated SUM-159B1KO cells (Figure 6A, 6B, Supplementary Fig 7E). By comparison, the level of aberrant mitoses was only 20% in SUM-159B1WT (Figure 6B).

Micronuclei in SUM-159B1KO are linked to acute replicative stress and sensed by cGAS

MN formation is linked to lagging mitotic chromosomes resulting from non-resolved genomic damage (27). Remarkably, we noted that MN in SUM-159B1KO presented both pan-nuclear γH2AX and strong non-denaturing BrdU staining, indicating they encompassed long stretches of ssDNA (Figure 6C). Due to the observed impact of MRE11 inhibition on ssDNA accumulation in SUM-159B1KO, we tested whether mirin treatment also affected MN formation. Mirin treatment reduced MN numbers by 53% in SUM-159B1KO, but showed a more limited effect in SUM-159B1WT (Figure 6D, 6E). It has been reported that mitotic bridges and MN may be sensed by cyclic GMP-AMP synthase (cGAS), possibly due to cytoplasmic DNA exposure (27),(28), (29). Accordingly, we noted that, in gemcitabine-treated SUM159B1KO, DNA bridges and up to 30% BrdU-positive micronuclei presented a clear cGAS signal (Figure 6F, 6G). By contrast, the cGAS signal was significantly less prevalent in the few MN detected in SUM159B1WT (Figure 6H).

Our data, thus, indicate that BRCA1-deficient cells undergoing replication catastrophe slip into

mitosis and produce MN associated with a strong cGAS signal.

Gemcitabine responsive TNBC PDX show increased γH2AX and cGAS staining

The strong increase in γH2AX levels assorted to pan-nuclear staining observed in cell models undergoing massive ssDNA accumulation incited us to verify whether γH2AX staining levels might be related to gemcitabine sensitivity in breast cancer patient derived xenograft (PDX) models. We, thus, selected three TNBC PDX models whose BRCA1 statuses had been determined in a previous work (16). We selected one *BRCA1*WT PDX (b3804) and two models showing hypermethylation of the *BRCA1* promoter region (15b0018 and b4122). Interestingly, both 15b0018 and b4122 showed loss of BRCA1 protein expression. However, while b4122 presented impaired RAD51 nuclear foci formation and responded positively to olaparib-treatment, 15b0018 produced RAD51 foci and responded poorly to olaparib (16). We determined sensitivity of these three models to two injections per week of 50mg/kg gemcitabine for four weeks. Interestingly, while PDX 15b0018 progressed under gemcitabine-treatment and b3804 was stabilized, the BRCA1-deficient b4122 clearly regressed within the four weeks of this treatment (Figure 7A-7C). The day after the last drug injection residual tumors were sampled and immunolabeled for γH2AX and cGAS expression. γH2AX and cGAS positive cells were quantified in gemcitabine and mock-treated tumor sections. γH2AX and cGAS positive cell numbers were highest in PDX b4122, which responded best to gemcitabine. These numbers were lowest in PDX 15b0018 (Figure 7D-G). Notably, while the growth of PDX b3804 was stabilized under gemcitabine treatment, it showed intermediate γH2AX and distinctly lower cGAS staining levels (Figure 7E-7G). These *in vivo* data are, thus, consonant with our cell culture model observations and suggest that elevated sensitivity to gemcitabine treatment could be marked by increased γH2AX and cGAS staining.

Discussion

Here we show that, upon gemcitabine treatment, *BRCA1*-deficient models encounter massive ssDNA accumulation and elevated cell death, in comparison with their BRCA1-proficient counterparts. Because these cells showed strong and persistent imbalance of γH2AX- and RPA-positive cells, this process was reminiscent of replication catastrophe, which is an acute and lethal form of replication stress, originally described in association with ATR impairment (20). Replication catastrophe was proposed to result from an excess of ssDNA accumulation, which titrates available RPA in the cell and causes severely impaired protection of stalled replication forks (20). By contrast, *BRCA1*-proficient models only showed transient γH2AX/RPA imbalance and modest mortality. Furthermore, we report, for what we believe is the first time, that a substantial fraction of gemcitabine-treated *BRCA1*-deficient cells massively accumulate ssDNA in the absence of concomitant RPA and/or RAD51 signals. Remarkably, the number of cells exhibiting this phenotype increased over time, rising up to 70% of cells 48h after drug removal. These results suggest that ssDNA levels produced in gemcitabine-treated BRCA1-deficient models exceed those required for RPA titration, and are the result of further events. The fact that MRE11 siRNA attenuation or treatment with the MRE11 inhibitors mirin or PFM39 induced a strong reduction of ssDNA levels in gemcitabine-treated SUM-159B1KO cells, clearly indicates the leading role of uncontrolled resection by MRE11 in this context. MRE11 resection of nascent strands has been proposed to be associated with replication fork reversal, but could also occur at other structure bearing nascent DNA (12), (30), (31). However, replication fork reversal produces nascent DNA overhangs in response to acute replication fork stalling (23). In *BRCA*-deficient cells, these structures are particularly vulnerable to resection due the absence or limited availability of RAD51 (12), (13), (18), (24), (25). Interestingly, we show that gemcitabine-treated *BRCA1*-deficient cells present elevated levels of nuclear SMARCAL1, possibly suggesting increased fork reversal. However, in the absence of electron-microscopy assessment, no definite conclusion can be reached on replication fork reversal in our system (32). It must also be acknowledged that MRE11 is insufficiently processive to support resection of long DNA stretches, requiring the involvement of EXO1 and/or WRN/DNA2 exonucleases (25), (33). MRE11 recruitment to nascent DNA stretches would, therefore, appear to act as a priming event. Interestingly, recent findings have shown that MRE11 binds to gemcitabine incorporated into the nascent DNA strand in order to actively remove it, further supporting the central role of MRE11 in gemcitabine-treated *BRCA1*-deficient models (34).

By contrast, 24h treatment with 100μM olaparib did not result in mirin sensitive ssDNA accumulation in SUM-159B1KO cells. It is of note that DNA synthesis repriming rather than fork reversal is preferentially activated by olaparib or other PARPi treatment (22), (35). We further noted that,

while no RAD51 nor RPA signals were detected, 53BP1 foci numbers were increased significantly in gemcitabine-treated *BRCA1*-deficient cells. There was a marked increase in 53BP1 foci in *BRCA1*-deficient cells showing intense pan-nuclear γH2AX staining, instead of discrete γH2AX foci. This strong increase in 53BP1 signals in pan-nuclear γH2AX staining cells was fully coherent with increased levels of DNA breaks revealed by PFGE. Interestingly, the number of cells showing this phenotype increased dramatically between 24 and 48h after drug removal. By contrast, BrdU-positive cell numbers increased steadily between 8 and 48h, suggesting that pan-nuclear γH2AX staining could represent a late, possibly final, stage of acute replication stress. The shift from γH2AX foci to pan-nuclear staining may indicate massive DNA breakage resulting from replication fork breakdown and, as such correspond, as previously proposed (36), to a pre-apoptotic signal. Our data show that addition of Z-VAD to gemcitabine-treated SUM-159B1KO strongly reduced pan-nuclear γH2AX staining cell numbers support a link with apoptosis (Supplementary Fig 4B). This led us to question whether the level of γH2AX staining in gemcitabine-treated PDX TNBC models could reflect their sensitivity to the drug. Our analysis indicated that γH2AX levels were indeed increased, both in terms of positive cell numbers and staining intensity, in PDX models responding best to gemcitabine. These results suggest that the intensity and pattern of γH2AX staining in post-treatment patient biopsies could be informative as to the responsiveness of a tumor to replication poisons. However, this conclusion will need to be verified in larger cohorts of PDX models and patient biopsies. Interestingly, despite robust ssDNA accumulation, *BRCA1*-deficient TNBC cells suffering from acute replication stress reached M phase and produced aberrant mitoses, particularly, micronuclei (MN) showing intense BrdU labeling. It is therefore interesting that MRE11 inhibition reduced BrdU-positive MN numbers. It is, hence, most likely that the BrdU-positive MN originated from lagging chromosomes bearing long stretches of ssDNA (37). The presence of chromatin bridges in the aberrant mitotic fields of gemcitabine-treated SUM159-B1KO cells supports this hypothesis. In addition, we noted that BrdU and γH2AX labeled MN also presented a strong signal of the cytoplasmic DNA sensor cGAS. Similarly, we noted that the PDX model responding best to gemcitabine treatment also presented clear cGAS staining. Cyclic GMP–AMP synthase (cGAS) is a component of the innate immune system (38), frequently activated in tumor cells and shown to react with MN (27),(28). However, it is of note that we could not clearly identify innate immunity activation in our system downstream of cGAS sensing. However, recent works have shown that cGAS sensing of MN was not necessarily associated with STING, TBK1 or IRF3 innate immunity activation (29), but could result from nucleosome displacement by MRE11 as part of ZBP1-RIPK3-MLKL-mediated necroptosis (39). Hence, our data suggest that gemcitabine treatment of BRCA-deficient TNBC could be beneficial to patients due its strong impact on tumor cell survival.

Author contribution

Imene Tabet; Conceptualization, investigation, validation, methodology, drafting and editing the paper. Esin Orhan; investigation, validation, methodology, editing the draft. Ermes Candiello; Conceptualization, investigation, editing the draft. Carolina Velazquez; investigation, data curation, validation, methodology. Lise Fenou; resources, validation, data curation, methodology. Beatrice Orsetti; methodology, resources. Geneviève Rodier; methodology, validation, editing the draft. William Jacot; resources, editing the draft. Cyril Ribeyre; investigation, data curation, validation, methodology, editing the draft. Claude Sardet; funding acquisition, supervision, editing the draft. Charles Theillet; Conceptualization, Supervision and coordination, writing and editing the paper, funding acquisition,

Acknowledgements

The authors sincerely acknowledge Dr Philippe Pasero (IGH) and Dr Isabelle Jariel (IRCM) for their fruitful discussions during the course of this work and constructive comments on the manuscript. Furthermore, sincere thanks are due to the staffs of the animal facility at IRCM for their constant support and expert help.

Grants and financial support

This work benefited from the following financial support: Institutional support from the Institut National de la Santé et de la Recherche Médicale, Astra-Zeneca contract # 2018-02069, Institut National du Cancer PRTK-2017 MODUREPOIS, Ligue Nationale Contre le Cancer 'Comité régional Occitanie-Est' 2021-R22031FF and the SIRIC Montpellier Cancer Grant INCa-DGOS-Inserm_12553, LabMuse Epigenmed METABOHOX from the University of Montpellier.

Author information

Ermes Candielo, present address; MBC-DBMSS Institute – IRCCS, Torino, Italy.
Carolina Velazquez, present address; Gynecological Oncology Laboratory, Department of Oncology, KU Leuven and Leuven Cancer Institute (LKI), 3000 Leuven, Belgium.

References

{papers2_bibliography}

1. Lord CJ, Ashworth A. BRCAness revisited. Nature Publishing Group. 2016;16:110–20.

2. Kolinjivadi AM, Sannino V, De Antoni A, Zadorozhny K, Kilkenny M, Técher H, et al. Smarcal1-Mediated Fork Reversal Triggers Mre11-Dependent Degradation of Nascent DNA in the Absence of Brca2 and Stable Rad51 Nucleofilaments. Molecular Cell. 2017;67:867–7.

3. Quinet A, Tirman S, Jackson J, Šviković S, Lemaçon D, Carvajal-Maldonado D, et al. PRIMPOL-Mediated Adaptive Response Suppresses Replication Fork Reversal in BRCA-Deficient Cells. Molecular Cell. 2020;77:461–9.

4. Daboussi F, Courbet S, Benhamou S, Kannouche P, Zdzienicka MZ, Debatisse M, et al. A homologous recombination defect affects replication-fork progression in mammalian cells. Journal of Cell Science. 2008;121:162–6.

5. Wilhelm T, Ragu S, Magdalou I, Machon C, Dardillac E, Técher H, et al. Slow

Replication Fork Velocity of Homologous Recombination-Defective Cells Results from Endogenous Oxidative Stress. Maizels N, editor. 2016;12:e1006007–20.

6. Zeman MK, Cimprich KA. Causes and consequences of replication stress. Nat Cell Biol. 2014;16:2–9.

7. Couch FJ, Hart SN, Sharma P, Toland AE, Wang X, Miron P, et al. Inherited Mutations in 17 Breast Cancer Susceptibility Genes Among a Large Triple-Negative Breast Cancer Cohort Unselected for Family History of Breast Cancer. Journal of Clinical Oncology. 2015;33:304–11.

8. Jacot W, Lopez-Crapez E, Mollevi C, Boissière-Michot F, Simony-Lafontaine J, Ho-Pun-Cheung A, et al. BRCA1 Promoter Hypermethylation is Associated with Good Prognosis and Chemosensitivity in Triple-Negative Breast Cancer. Cancers (Basel). 2020;12.

9. Maisano R, Zavettieri M, Azzarello D, Raffaele M, Maisano M, Bottari M, et al. Carboplatin and gemcitabine combination in metastatic triple-negative anthracycline- and taxane-pretreated breast cancer patients: a phase II study. J Chemother. 2011;23:40–3.

10. Hawryłkiewicz A, Ptaszyńska N. Gemcitabine Peptide-Based Conjugates and Their Application in Targeted Tumor Therapy. Molecules. 2021;26.

11. Buis J, Wu Y, Deng Y, Leddon J, Westfield G, Eckersdorff M, et al. Mre11 nuclease activity has essential roles in DNA repair and genomic stability distinct from ATM activation. Cell. 2008;135:85–96.

12. Schlacher K, Christ N, Siaud N, Egashira A, Wu H, Jasin M. Double-Strand Break Repair-Independent Role for BRCA2 in Blocking Stalled Replication Fork Degradation by MRE11. Cell. 2011;145:529–42.

13. Mijic S, Zellweger R, Chappidi N, Berti M, Jacobs K, Mutreja K, et al. Replication fork reversal triggers fork degradation in BRCA2-defective cells. Nat Comms. 2017;8:859.

14. Orhan E, Velazquez C, Tabet I, Fenou L, Rodier G, Orsetti B, et al. CDK inhibition results in pharmacologic BRCAness increasing sensitivity to olaparib in BRCA1-WT and olaparib resistant in Triple Negative Breast Cancer. Cancer Lett. 2024;589:216820.

15. Manoir du S, Orsetti B, Bras-Gonçalves R, Nguyen T-T, Lasorsa L, Boissière F, et al. Breast tumor PDXs are genetically plastic and correspond to a subset of aggressive cancers prone to relapse. Molecular Oncology. 2014;8:431–43.

16. Velazquez C, Orhan E, Tabet I, Fenou L, Orsetti B, Adélaïde J, et al. BRCA1-methylated triple negative breast cancers previously exposed to neoadjuvant chemotherapy form RAD51 foci and respond poorly to olaparib. Frontiers in Oncology. 2023;13:1125021.

17. Elstrodt F, Hollestelle A, Nagel JHA, Gorin M, Wasielewski M, van den Ouweland A, et al. BRCA1 mutation analysis of 41 human breast cancer cell lines

reveals three new deleterious mutants. Cancer Res. 2006;66:41–5.

18. Hashimoto Y, Ray Chaudhuri A, Lopes M, Costanzo V. Rad51 protects nascent DNA from Mre11-dependent degradation and promotes continuous DNA synthesis. Nat Struct Mol Biol. 2010;17:1305–11.

19. Mirman Z, de Lange T. 53BP1: a DSB escort. Genes & Development. 2020;34:7–23.

20. Toledo LI, Altmeyer M, Rask M-B, Lukas C, Larsen DH, Povlsen LK, et al. ATR prohibits replication catastrophe by preventing global exhaustion of RPA. Cell. 2013;155:1088–103.

21. Costanzo V. Brca2, Rad51 and Mre11: performing balancing acts on replication forks. DNA Repair. 2011;10:1060–5.

22. Panzarino NJ, Krais JJ, Cong K, Peng M, Mosqueda M, Nayak SU, et al. Replication Gaps Underlie BRCA Deficiency and Therapy Response. Cancer Res. 2021;81:1388–97.

23. Zellweger R, Dalcher D, Mutreja K, Berti M, Schmid JA, Herrador R, et al. Rad51-mediated replication fork reversal is a global response to genotoxic treatments in human cells. J Cell Biol. 2015;208:563–79.

24. Thangavel S, Berti M, Levikova M, Pinto C, Gomathinayagam S, Vujanovic M, et al. DNA2 drives processing and restart of reversed replication forks in human cells. J Cell Biol. 2015;208:545–62.

25. Lemaçon D, Jackson J, Quinet A, Brickner JR, Li S, Yazinski S, et al. MRE11 and EXO1 nucleases degrade reversed forks and elicit MUS81-dependent fork rescue in BRCA2-deficient cells. Nat Comms. 2017;8:860.

26. Warren NJH, Eastman A. Inhibition of checkpoint kinase 1 following gemcitabine-mediated S phase arrest results in CDC7- and CDK2-dependent replication catastrophe. J Biol Chem. 2019;294:1763–78.

27. Flynn PJ, Koch PD, the TMPO, 2021. Chromatin bridges, not micronuclei, activate cGAS after drug-induced mitotic errors in human cells. National Acad Sciences.

28. Mackenzie KJ, Carroll P, Martin C-A, Murina O, Fluteau A, Simpson DJ, et al. cGAS surveillance of micronuclei links genome instability to innate immunity. Nature. 2017;548:461–5.

29. Takaki T, Millar R, Hiley CT, Boulton SJ. Micronuclei induced by radiation, replication stress, or chromosome segregation errors do not activate cGAS-STING. Molecular Cell. 2024;84:2203–5.

30. Quinet A, Lemaçon D, Vindigni A. Replication Fork Reversal: Players and Guardians. Molecular Cell. 2017;68:830–3.

31. Tirman S, Quinet A, Wood M, Meroni A, Cybulla E, Jackson J, et al. Temporally

distinct post-replicative repair mechanisms fill PRIMPOL-dependent ssDNA gaps in human cells. Molecular Cell. 2021;81:4026–8.

32. Saldivar JC, Cortez D, Cimprich KA. The essential kinase ATR: ensuring faithful duplication of a challenging genome. Nat Rev Mol Cell Biol. 2017;18:622–36.

33. Berti M, Cortez D, Lopes M. The plasticity of DNA replication forks in response to clinically relevant genotoxic stress. Nat Rev Mol Cell Biol. 2020;21:633–51.

34. Boeckemeier L, Kraehenbuehl R, Keszthelyi A, Gasasira MU, Vernon EG, Beardmore R, et al. Mre11 exonuclease activity removes the chain-terminating nucleoside analog gemcitabine from the nascent strand during DNA replication. Sci Adv. 2020;6:eaaz4126.

35. Cong K, Peng M, Kousholt AN, Lee WTC, Lee S, Nayak S, et al. Replication gaps are a key determinant of PARP inhibitor synthetic lethality with BRCA deficiency. Molecular Cell. 2021;81:3128–3144.e7.

36. Moeglin E, Desplancq D, Conic S, Oulad-Abdelghani M, Stoessel A, Chiper M, et al. Uniform Widespread Nuclear Phosphorylation of Histone H2AX Is an Indicator of Lethal DNA Replication Stress. Cancers (Basel). 2019;11:355–22.

37. Hoffelder DR, Luo L, Burke NA, Watkins SC, Gollin SM, Saunders WS. Resolution of anaphase bridges in cancer cells. Chromosoma. 2004;112:389–97.

38. Motwani M, Pesiridis S, Fitzgerald KA. DNA sensing by the cGAS-STING pathway in health and disease. Nat Rev Genet. 2019;20:657–74.

39. Cho M-G, Kumar RJ, Lin C-C, Boyer JA, Shahir JA, Fagan-Solis K, et al. MRE11 liberates cGAS from nucleosome sequestration during tumorigenesis. Nature. 2024;625:585–92.

Figure Legends

Figure 1: BRCA1-deficiency is associated with accrued gemcitabine mortality and absence of HR response A: cell viability in response to increasing concentrations of gemcitabine, BRCA1-proficient cell lines are shown in black curves and BRCA1-deficient in red. HCC-38 whose status is intermediate is depicted in grey. **B**: cell mortality of gemcitabine treated SUM159B1WT (black) and SUM159B1KO (red) cells. Cell death upon treatment with 100nM gemcitabine was assessed by FACS quantification and combines AnnexinV+ and propidium iodide+ cells. **C**: treatment protocol applied here; cells were exposed to the drug for 24h, then left to recover in fresh medium for 48h before mortality was measured. **D, E**: immunofluorescence analysis and quantification of BRCA1, BRCA2, RAD51 and 53BP1 nuclear foci formation in SUM-159B1WT cells upon gemcitabine treatment. **F, G:** same as D, E but with SUM-159B1KO cells. Cells presenting more than 10 nuclear foci by immunofluorescence were scored positive and at least 300 cells were scored per slide. Boxes with dotted lines in the merge images correspond to magnification of typical nuclei. Statistical significance was assessed using the non-parametric Student t-test. P-values were considered as significant when *, ≤ 0.05 and

highly significant when **, ≤ 0.01; ***, ≤ 0.005. White bars at the bottom of microscopy image indicate the scale: 20µm.

Figure 2: Gemcitabine treatment induces severe and persitent replication stress in BRCA1-deficient cell models. A, B: FACS analysis quantification of γH2AX-positive and RPA-positive cell fractions in SUM-159B1 (BRCA1-proficient) (A) and SUM-159B1KO (BRCA1-deficient) (B), note the imbalance between γH2AX- and RPA-positive cell numbers. **C, D:** SUM-159B1 showed no γH2AX/RPA imbalance in immunofluorescence (IF) analyses. Selected immunofluorescence sections of SUM-159B1WT stained with anti-γH2AX (red) and RPA (green) antibodies (C) and quantification of γH2AX-positive and RPA-positive cells by IF (D). **E, F:** SUM-159B1KO showed strong γH2AX/RPA imbalance by IF. Selected immunofluorescence sections stained with anti-γH2AX (red) and RPA (green) antibodies (E) and quantification of γH2AX-positive and RPA-positive cells by IF (F). At least 300 cells were scored per slide. Boxes with dotted lines in the merge images correspond to magnification of typical nuclei. Scale bars: 20µm.

Figure 3: cells undergoing replication catastrophe are characterized by intense non-denaturing BrdU labelling, absence of RPA signal and pan-nuclear γH2AX staining. A: examples of BrdU and RPA32 immunofluorescence staining in SUM-159B1WT**. B**: quantification of BrdU-positive cells in SUM-159B1WT and SUM-159B1KO at different time lapses post gemcitabine removal**. C**: examples of BrdU and RPA32 immunofluorescence staining in SUM-159B1KO. Yellow circles indicate cells showing no RPA signal while staining intensely for BrdU **D:** quantification of BrdU-positive and RPA32-negative cells in SUM-159B1WT and SUM-159B1KO **E:** examples of BrdU-positive and pan-nuclear γH2AX staining cells in SUM-159B1WT 48H after drug removal. **F:** same as E in SUM-159B1KO. **G:** quantification of the fraction of pan-nuclear γH2AX staining cells showing no RPA32 signal in SUM-159B1WT and SUM-159B1KO. Boxes with dotted lines in the merge images correspond to magnification of typical nuclei. Statistical significance was assessed using the non-parametric Student t-test. P-values were considered significant when *, ≤ 0.05 and highly significant **, ≤ 0.01; ***, ≤ 0.005. Scale bars: 20µm.

Figure 4: SUM159B1KO cells with pan-nuclear γH2AX staining show no RAD51 foci, but strong 53BP1 signals. A: examples of γH2AX and RPA32 immunostaining staining 48H after drug removal. **B:** quantification of pan-nuclear γH2AX+/RAP32+ cells in SUM-159B1WT and SUM-159B1KO at 24h and 48h after drug removal. **C:** BRCA1, RPA32 and γH2AX protein expression levels by western blot in SUM-159B1WT and SUM-159B1KO cells treated or not with gemcitabine for 24h. **D:** western blot analysis of cytoplasmic (Cyt) and chromatin (Chr) protein extracts in SUM-159B1WT and SUM-159B1KO cells treated or not with gemcitabine for 24h/48h. H3 corresponds to histone H3 used here as a subcellular fractionation control. **E:** examples of γH2AX and RAD51 immunofluorescence staining 48H after drug removal. **F:** quantification of pan-nuclear γH2AX+/RAD51- cells in SUM-159B1WT and SUM-159B1KO. **E:** examples of γH2AX and 53BP1 immunostaining. **F:** quantification of pan-nuclear γH2AX+/53BP1+ cells in SUM-159B1WT and SUM-159B1KO. Quantification was performed on at least 300 cells per section for each antibody. Boxes with dotted lines in the merge images correspond to magnification of typical nuclei. Statistical significance was assessed using the non-parametric Student t-test. P-values were considered as significant when *, ≤ 0.05 and highly significant when **, ≤ 0.01; ***, ≤ 0.005. Scale bars: 20µm.

Figure 5: MRE11 is instrumental for ssDNA accumulation and onset of replication catastrophe in gemcitabine treated BRCA1-deficient cells. A, B, C: impact of mirin treatment on the number of BrdU and γH2AX positive cells in gemcitabine treated SUM-159B1WT. γH2AX and BrdU immunofluorescence staining in cells treated for 24h with Gemcitabine (top row) and 100nM Gemcitabine + 50µM mirin (bottom row) (A). Quantification of BrdU+ cells in the different conditions (B). Quantification of γH2AX+ cells (C). **D, E, F:** impact of mirin treatment on the number of BrdU and

γH2AX positive cells in gemcitabine treated SUM-159B1KO. γH2AX and BrdU immunofluorescence staining in cells treated with Gemcitabine (top row) and Gemcitabine + mirin (bottom row) (D). Quantification of BrdU+ cells in the different conditions (E). Quantification of γH2AX+ cells (F). **G:** quantification of DSB breaks in SUM-159B1WT (black bars) and SUM-159B1KO (red bars) treated with gemcitabine +/- 50µM mirin. **H:** quantification of DSB breaks in SUM-159B1WT and SUM-159B1KO treated with gemcitabine +/- 50µM Z-VAD. PFGE analysis was performed on cells collected 48h after gemcitabine removal **I, J, K:** impact of mirin treatment on the number of BrdU and γH2AX positive cells in olaparib treated SUM-159B1WT cells. γH2AX and BrdU immunofluorescence staining in cells treated for 24h with 100 µM olaparib (top row) and 100 µM olaparib + 50µM mirin (bottom row) (I). Quantification of BrdU+ cells in the different conditions (J). Quantification of γH2AX+ cells (K). **L, M, N:** same as I, J, K in SUM-159B1KO cells**.** Boxes with dotted lines in the merge images correspond to magnification of typical nuclei. Statistical significance was assessed using the non-parametric Student t-test. P-values were considered as significant when *, ≤0.05 and highly significant when **, ≤0.01; ***, ≤0.005; ****, ≤0.001**.** Scale bars: 20µm**.**

Figure 6: BRCA1-deficient cells undergoing replication catastrophe produce aberrant mitoses and cGAS-positive micronuclei. A: examples of aberrant mitotic figures in synchronized SUM-159B1KO cells treated with gemcitabine. **B:** fraction of aberrant mitoses in gemcitabine treated cells. Red SUM-159B1KO, black SUM-159B1WT. **C:** in SUM-159KO micronuclei are BrdU and γH2AX-positive. **D, E:** impact of 50µM mirin treatment on micronuclei numbers in gemcitabine-treated SUM-159B1 and SUM-159B1KO respectively. **F:** mitotic DNA bridges stain positive for cGAS in gemcitabine-treated SUM-159B1KO **G:** γH2AX+ micronuclei show cGAS staining in gemcitabine-treated SUM-159B1KO. **H:** quantification cGAS-positive micronuclei in SUM-159B1WT and SUM-159B1KO. Statistical significance was assessed using the non-parametric Student t-test. P-values were considered as significant when *, ≤ 0.05 and highly significant when **, ≤ 0.01; ***, ≤ 0.005. Scale bars : 10µm in panels A and C and top panel F and G, 20µm in C lower panel.

Figure 7: TNBC PDX showing good response to gemcitabine exhibit increased γH2AX and cGAS staining. A, B, C: growth curves of PDX b3804, b15b0018 and b4122; black lines mock, red lines gemcitabine-treated. About 50mm3 of tumors were grafted subcutaneously to 8 mice in each experimental arm and treatment started when tumor volume had reached 150mm3 on average. Two injections/week of 50mg/kg gemcitabine were administered by IP injection for 4 weeks. Mice in the control arms were injected with the vehicule. **D, E:** γH2AX immunostaining and quantification of positive cells. **F,G**: cGAS immunostaining and quantification of positive cells. Statistical significance was assessed using the non-parametric Student t-test. P-values were considered as significant when *, ≤ 0.05 and highly significant when **, ≤ 0.01; ***, ≤ 0.005 ; ****, ≤ 0.001. Scale bars: 50µm**.**

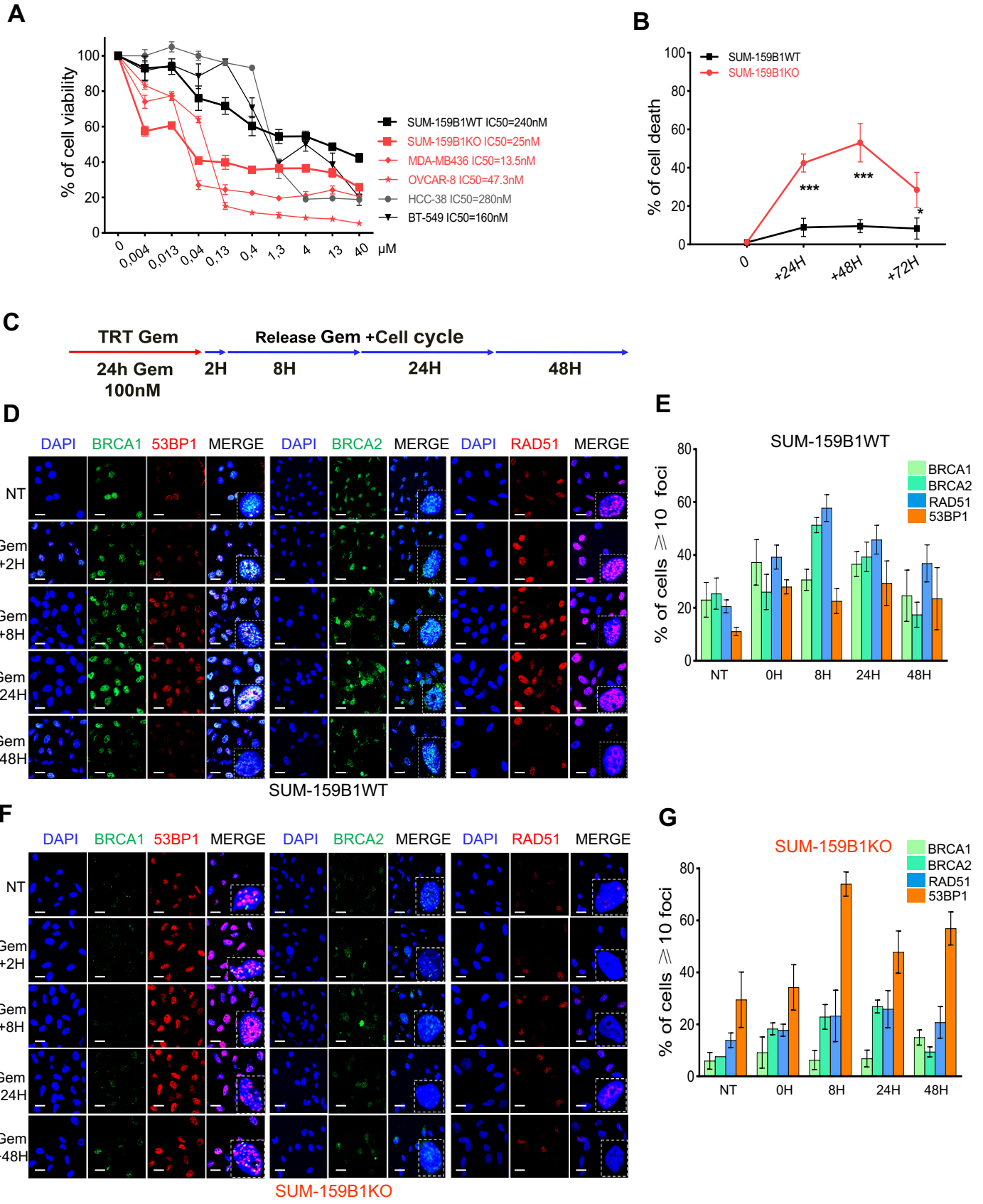
A
% of cell viability
SUM-159B1WT IC50=240nM
SUM-159B1KO IC50=25nM
MDA-MB436 IC50=13.5nM
OVCAR-8 IC50=47.3nM
HCC-38 IC50=280nM
BT-549 IC50=160nM
μM
B
% of cell death
SUM-159B1WT
SUM-159B1KO
C
TRT Gem
24h Gem 100nM
Release Gem +Cell cycle
2H
8H
24H
48H
D
DAPI BRCA1 53BP1 MERGE DAPI BRCA2 MERGE DAPI RAD51 MERGE
NT
Gem +2H
Gem +8H
Gem +24H
Gem +48H
SUM-159B1WT
E
SUM-159B1WT
% of cells ⩾ 10 foci
BRCA1
BRCA2
RAD51
53BP1
NT
0H
8H
24H
48H
F
DAPI BRCA1 53BP1 MERGE DAPI BRCA2 MERGE DAPI RAD51 MERGE
NT
Gem +2H
Gem +8H
Gem +24H
Gem +48H
SUM-159B1KO
G
SUM-159B1KO
% of cells ⩾ 10 foci
BRCA1
BRCA2
RAD51
53BP1
NT
0H
8H
24H
48H

Figure 1

Figure 1: BRCA1-deficiency is associated with accrued gemcitabine mortality and absence of HR response A: cell viability in response to increasing concentrations of gemcitabine, BRCA1-proficient cell lines are shown in black curves and BRCA1-deficient in red. HCC-38 whose status is intermediate is depicted in grey. **B**: cell mortality of gemcitabine treated SUM159B1WT (black) and SUM159B1KO (red) cells. Cell death was assessed by FACS quantification and combines AnnexinV+ and propidium iodide+ cells. **C**: treatment protocol applied here; cells were exposed to the drug for 24h, then left to recover in fresh medium for 48h before mortality was measured. **D, E**: immunofluorescence analysis and quantification of BRCA1, BRCA2, RAD51 and 53BP1 nuclear foci formation in SUM-159B1WT cells upon gemcitabine treatment. **F, G:** same as D, E but with SUM-159B1KO cells. Cells presenting more than 10 nuclear foci by immunofluorescence were scored positive and at least 300 cells were scored per slide. Boxes with dotted lines in the merge images correspond to magnification of typical nuclei. Statistical significance was assessed using the non-parametric Student t-test. P-values were considered as significant when *, ≤ 0.05 and highly significant when **, ≤ 0.01; ***, ≤ 0.005. White bars at the bottom of microscopy image indicate the scale: 20µm.

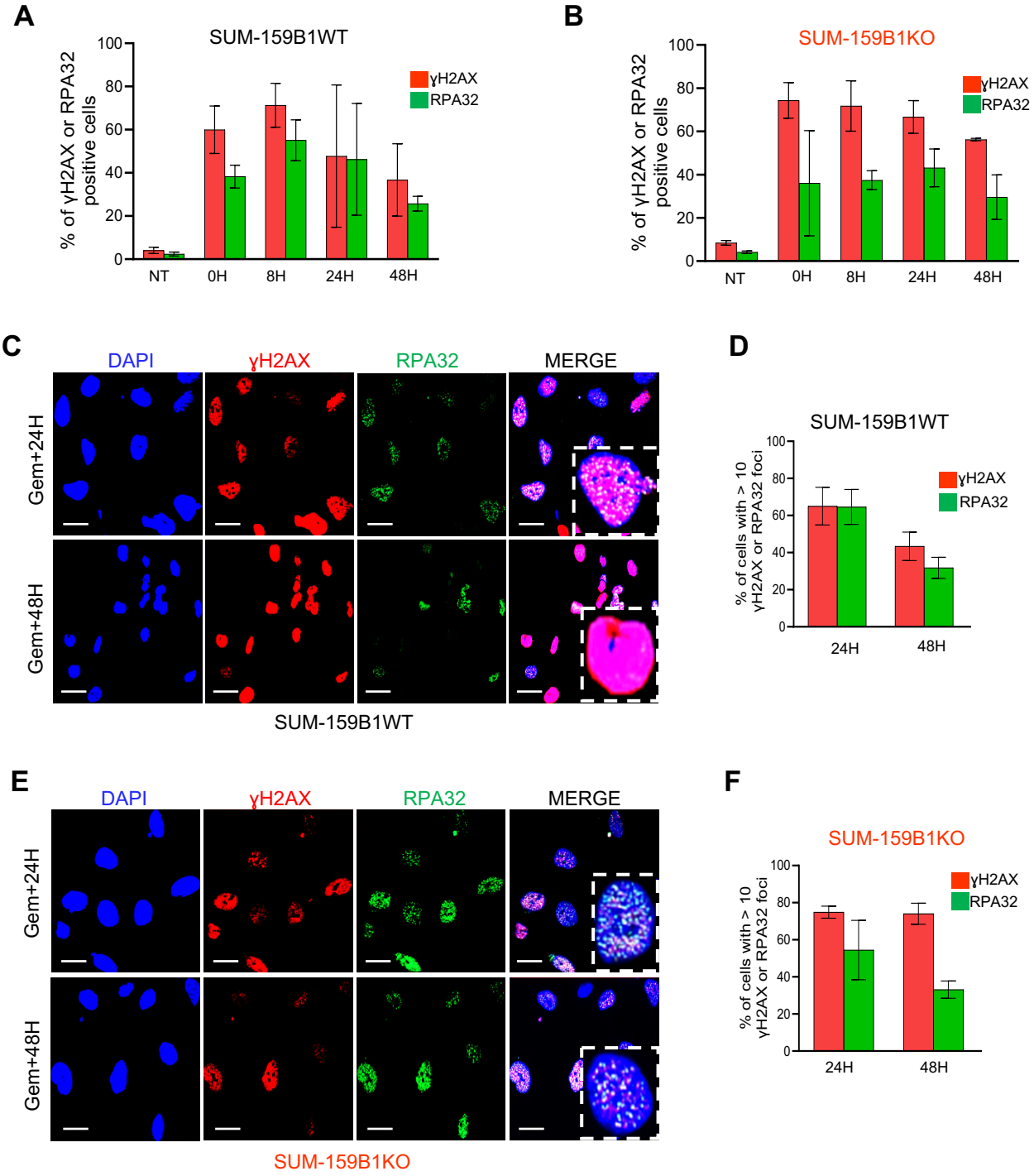

Figure 2

Figure 2

Figure 2: Gemcitabine treatment induces severe and persitent replication stress in BRCA1-deficient cell models. A, B: FACS analysis quantification of γH2AX-positive and RPA-positive cell fractions in SUM-159B1 (BRCA1-proficient) (A) and SUM-159B1KO (BRCA1-deficient) (B), note the imbalance between γH2AX- and RPA-positive cell numbers. **C, D:** SUM-159B1 showed no γH2AX/RPA imbalance in immunofluorescence (IF) analyses. Selected immunofluorescence sections of SUM-159B1WT stained with anti-γH2AX (red) and RPA (green) antibodies (C) and quantification of γH2AX-positive and RPA-positive cells by IF (D). **E, F:** SUM-159B1KO showed strong γH2AX/RPA imbalance by IF. Selected immunofluorescence sections stained with anti-γH2AX (red) and RPA (green) antibodies (E) and quantification of γH2AX-positive and RPA-positive cells by IF (F). At least 300 cells were scored per slide. Boxes with dotted lines in the merge images correspond to magnification of typical nuclei. Scale bars: 20μm.

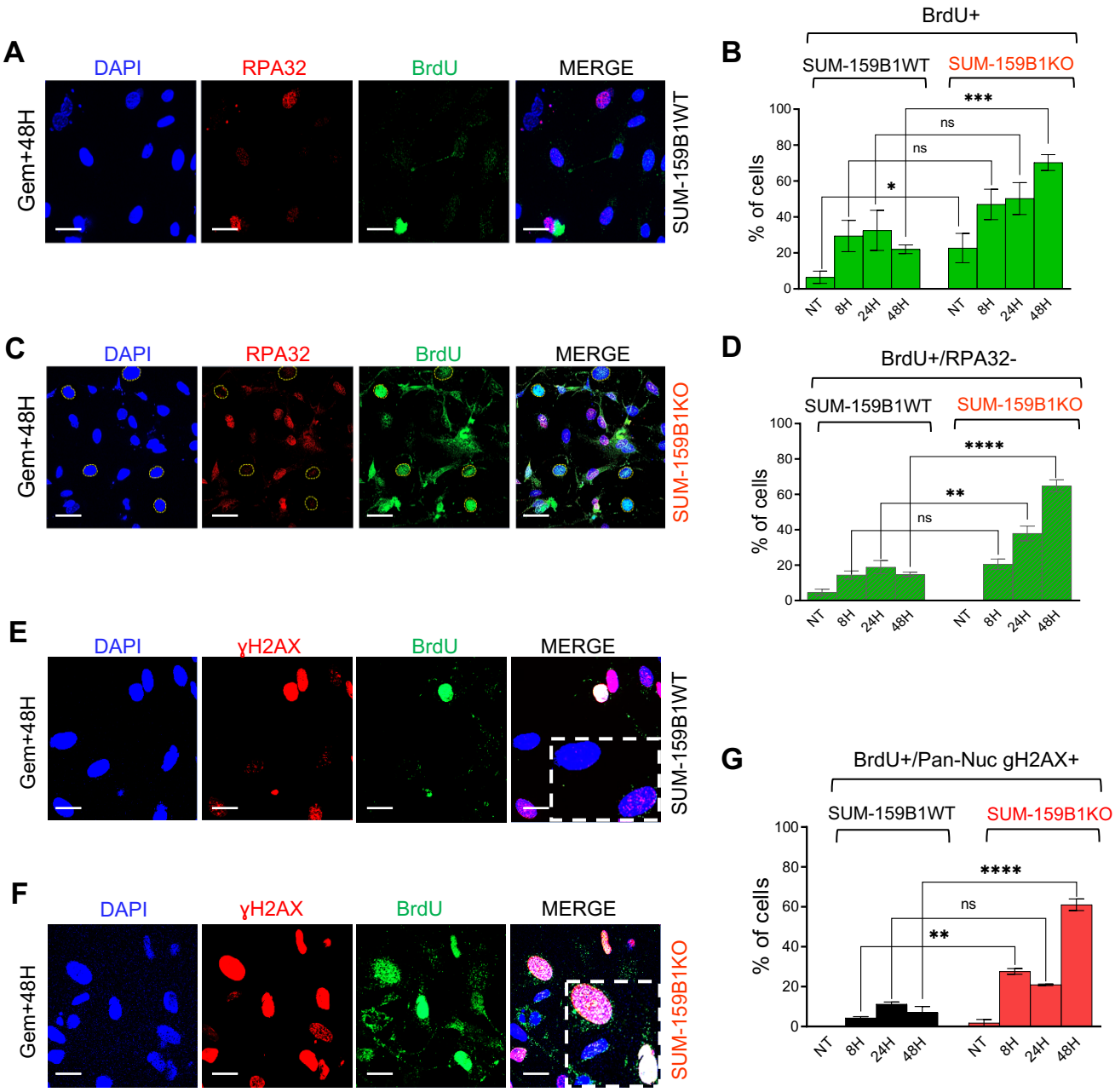
A
DAPI
RPA32
BrdU
MERGE
Gem+48H
SUM-159B1WT
B
BrdU+
SUM-159B1WT
SUM-159B1KO
% of cells
***
ns
ns
*
NT
8H
24H
48H
C
DAPI
RPA32
BrdU
MERGE
Gem+48H
SUM-159B1KO
D
BrdU+/RPA32-
SUM-159B1WT
SUM-159B1KO
% of cells
****
**
ns
E
DAPI
γH2AX
BrdU
MERGE
Gem+48H
SUM-159B1WT
F
DAPI
γH2AX
BrdU
MERGE
Gem+48H
SUM-159B1KO
G
BrdU+/Pan-Nuc gH2AX+
SUM-159B1WT
SUM-159B1KO
% of cells
****
ns
**

Figure 3

Figure 3: cells undergoing replication catastrophe are characterized by intense non-denaturing BrdU labelling, absence of RPA signal and pan-nuclear γH2AX staining. A: examples of BrdU and RPA32 immunofluorescence staining in SUM-159B1WT**. B**: quantification of BrdU-positive cells in SUM-159B1WT and SUM-159B1KO at different time lapses post gemcitabine removal**. C**: examples of BrdU and RPA32 immunofluorescence staining in SUM-159B1KO. Yellow circles indicate cells showing no RPA signal while staining intensely for BrdU **D:** quantification of BrdU-positive and RPA32-negative cells in SUM-159B1WT and SUM-159B1KO **E:** examples of BrdU-positive and pan-nuclear γH2AX staining cells in SUM-159B1WT 48H after drug removal. **F:** same as E in SUM-159B1KO. **G:** quantification of the fraction of pan-nuclear γH2AX staining cells showing no RPA32 signal in SUM-159B1WT and SUM-159B1KO. Boxes with dotted lines in the merge images correspond to magnification of typical nuclei. Statistical significance was assessed using the non-parametric Student t-test. P-values were considered significant when *, ≤ 0.05 and highly significant **, ≤ 0.01; ***, ≤ 0.005. Scale bars: 20μm.

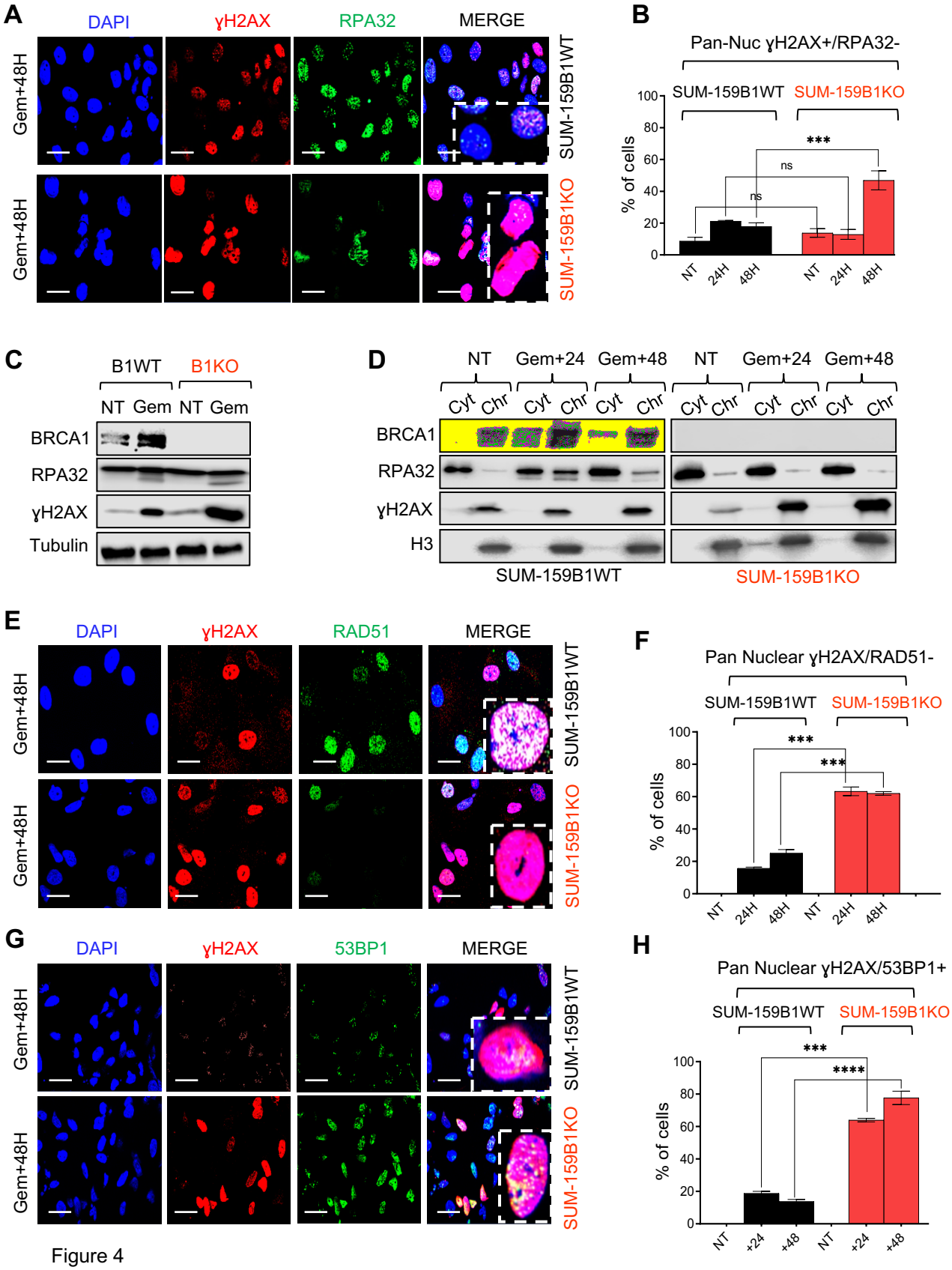
A
DAPI
γH2AX
RPA32
MERGE
Gem+48H
SUM-159B1WT
SUM-159B1KO
B
Pan-Nuc γH2AX+/RPA32-
SUM-159B1WT
SUM-159B1KO
% of cells
***
ns
NT
24H
48H
C
B1WT
B1KO
NT Gem NT Gem
BRCA1
RPA32
γH2AX
Tubulin
D
NT
Gem+24
Gem+48
Cyt
Chr
BRCA1
RPA32
γH2AX
H3
SUM-159B1WT
SUM-159B1KO
E
DAPI
γH2AX
RAD51
MERGE
F
Pan Nuclear γH2AX/RAD51-
****
G
DAPI
γH2AX
53BP1
MERGE
H
Pan Nuclear γH2AX/53BP1+
+24
+48

Figure 4

Figure 4: SUM159B1KO cells with pan-nuclear γH2AX staining show no RAD51 foci, but strong 53BP1 signals. A: examples of γH2AX and RPA32 immunostaining staining 48H after drug removal. **B:** quantification of pan-nuclear γH2AX+/RAP32+ cells in SUM-159B1WT and SUM-159B1KO at 24h and 48h after drug removal. **C:** BRCA1, RPA32 and γH2AX protein expression levels by western blot in SUM-159B1WT and SUM-159B1KO cells treated or not with gemcitabine for 24h. **D:** western blot analysis of cytoplasmic (Cyt) and chromatin (Chr) protein extracts in SUM-159B1WT and SUM-159B1KO cells treated or not with gemcitabine for 24h/48h. H3 corresponds to histone H3 used here as a subcellular fractionation control. **E:** examples of γH2AX and RAD51 immunofluorescence staining 48H after drug removal. **F:** quantification of pan-nuclear γH2AX+/RAD51- cells in SUM-159B1WT and SUM-159B1KO. **E:** examples of γH2AX and 53BP1 immunostaining. **F:** quantification of pan-nuclear γH2AX+/53BP1+ cells in SUM-159B1WT and SUM-159B1KO. Quantification was performed on at least 300 cells per section for each antibody. Boxes with dotted lines in the merge images correspond to magnification of typical nuclei. Statistical significance was assessed using the non-parametric Student t-test. P-values were considered as significant when *, ≤ 0.05 and highly significant when **, ≤ 0.01; ***, ≤ 0.005. Scale bars: 20μm.

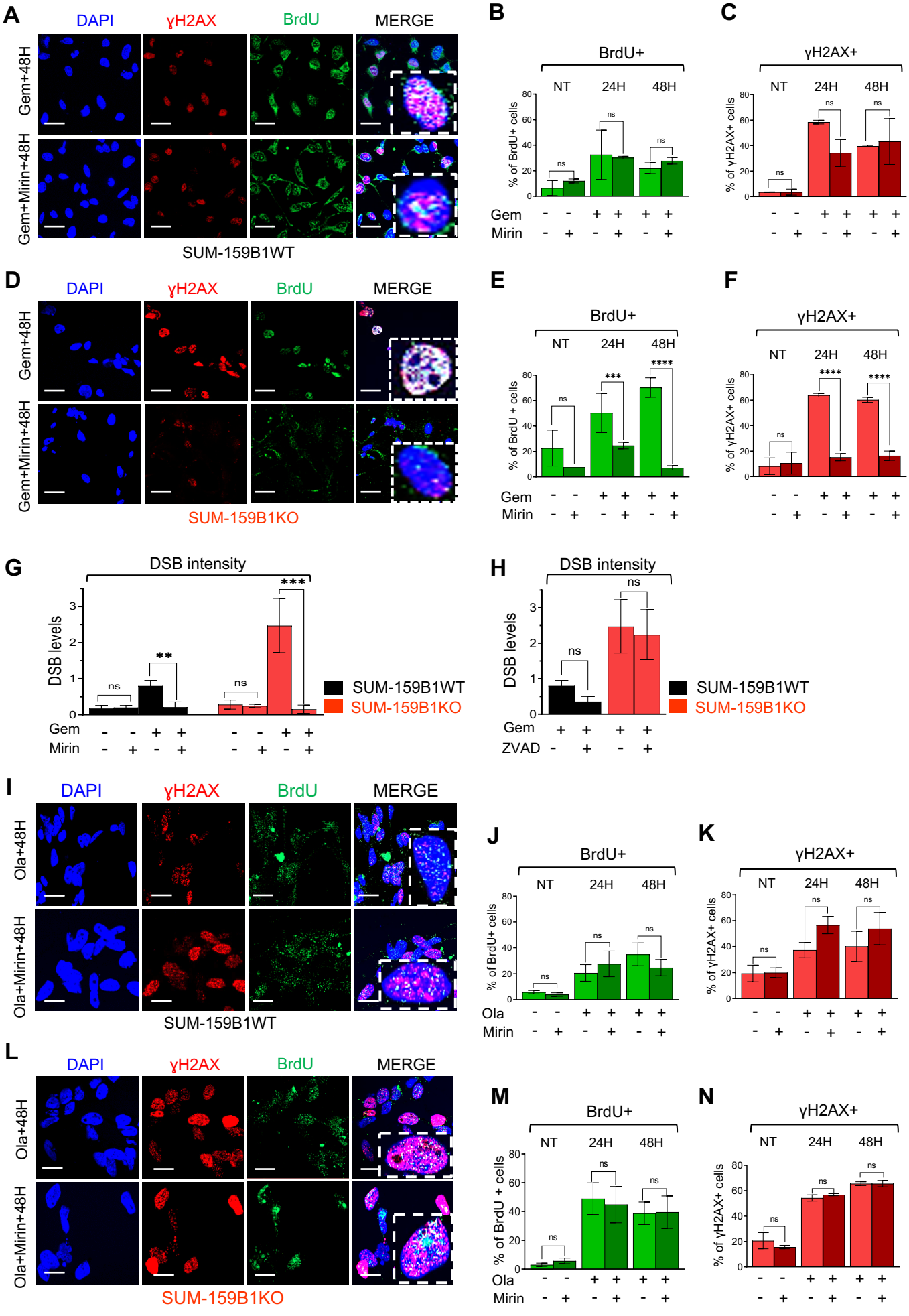
A
DAPI
γH2AX
BrdU
MERGE
Gem+48H
Gem+Mirin+48H
SUM-159B1WT
B
BrdU+
NT
24H
48H
% of BrdU+ cells
Gem
Mirin
C
γH2AX+
% of γH2AX+ cells
D
SUM-159B1KO
E
F
G
DSB intensity
DSB levels
SUM-159B1WT
SUM-159B1KO
H
ZVAD
I
Ola+48H
Ola+Mirin+48H
J
K
L
M
N

Figure 5

Figure 5: MRE11 is instrumental for ssDNA accumulation and onset of replication catastrophe in gemcitabine treated BRCA1-deficient cells. A, B, C: impact of mirin treatment on the number of BrdU and γH2AX positive cells in gemcitabine treated SUM-159B1WT. γH2AX and BrdU immunofluorescence staining in cells treated for 24h with Gemcitabine (top row) and 100nM Gemcitabine + 50µM mirin (bottom row) (A). Quantification of BrdU+ cells in the different conditions (B). Quantification of γH2AX+ cells (C). **D, E, F:** impact of mirin treatment on the number of BrdU and γH2AX positive cells in gemcitabine treated SUM-159B1KO. γH2AX and BrdU immunofluorescence staining in cells treated with Gemcitabine (top row) and Gemcitabine + mirin (bottom row) (D). Quantification of BrdU+ cells in the different conditions (E). Quantification of γH2AX+ cells (F). **G:** quantification of DSB breaks in SUM-159B1WT (black bars) and SUM-159B1KO (red bars) treated with gemcitabine +/- 50µM mirin. **H:** quantification of DSB breaks in SUM-159B1WT and SUM-159B1KO treated with gemcitabine +/- 50µM Z-VAD. PFGE analysis was performed on cells collected 48h after gemcitabine removal **I, J, K:** impact of mirin treatment on the number of BrdU and γH2AX positive cells in olaparib treated SUM-159B1WT cells. γH2AX and BrdU immunofluorescence staining in cells treated for 24h with 100 µM olaparib (top row) and 100 µM olaparib + 50µM mirin (bottom row) (I). Quantification of BrdU+ cells in the different conditions (J). Quantification of γH2AX+ cells (K). **L, M, N:** same as I, J, K in SUM-159B1KO cells**.** Boxes with dotted lines in the merge images correspond to magnification of typical nuclei. Statistical significance was assessed using the non-parametric Student t-test. P-values were considered as significant when *, ≤0.05 and highly significant when **, ≤0.01; ***, ≤0.005; ****, ≤0.001**.** Scale bars: 20µm.

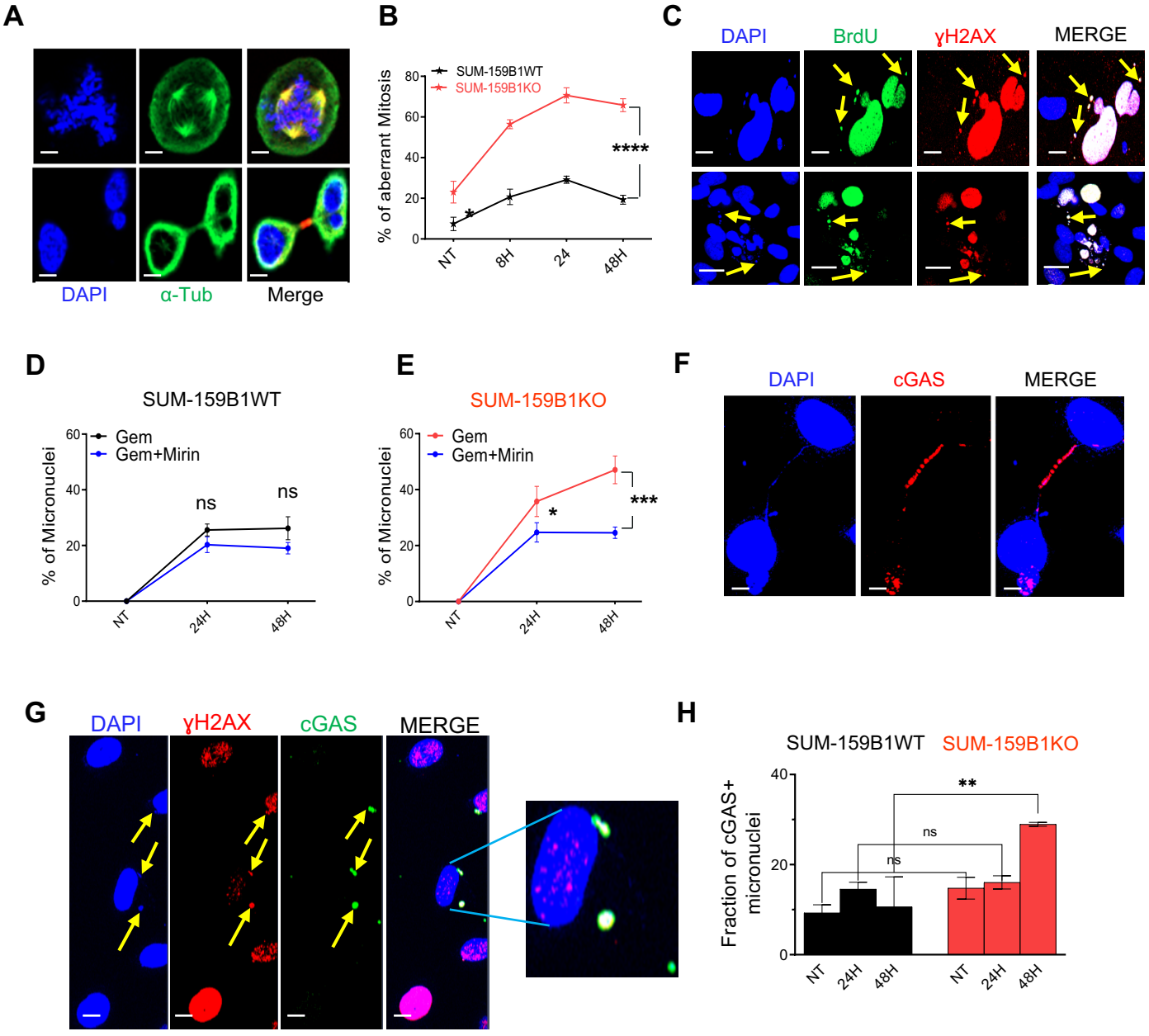
A
DAPI
α-Tub
Merge
B
SUM-159B1WT
SUM-159B1KO
% of aberrant Mitosis
****
NT
8H
24
48H
C
DAPI
BrdU
γH2AX
MERGE
D
SUM-159B1WT
Gem
Gem+Mirin
% of Micronuclei
ns
ns
NT
24H
48H
E
SUM-159B1KO
Gem
Gem+Mirin
% of Micronuclei
*
***
NT
24H
48H
F
DAPI
cGAS
MERGE
G
DAPI
γH2AX
cGAS
MERGE
H
SUM-159B1WT
SUM-159B1KO
Fraction of cGAS+ micronuclei
**
ns
ns
NT
24H
48H
NT
24H
48H

Figure 6

Figure 6: BRCA1-deficient cells undergoing replication catastrophe produce aberrant mitoses and cGAS-positive micronuclei. **A:** examples of aberrant mitotic figures in synchronized SUM-159B1KO cells treated with gemcitabine. **B:** fraction of aberrant mitoses in gemcitabine treated cells. Red SUM-159B1KO, black SUM-159B1WT. **C:** in SUM-159KO micronuclei are BrdU and γH2AX-positive. **D, E:** impact of 50μM mirin treatment on micronuclei numbers in gemcitabine-treated SUM-159B1 and SUM-159B1KO respectively. **F:** mitotic DNA bridges stain positive for cGAS in gemcitabine-treated SUM-159B1KO **G:** γH2AX+ micronuclei show cGAS staining in gemcitabine-treated SUM-159B1KO. **H:** quantification cGAS-positive micronuclei in SUM-159B1WT and SUM-159B1KO. Statistical significance was assessed using the non-parametric Student t-test. P-values were considered as significant when *, ≤ 0.05 and highly significant when **, ≤ 0.01; ***, ≤ 0.005. Scale bars : 10μm A, C upper pannel, F and G, 20μm C lower pannel.

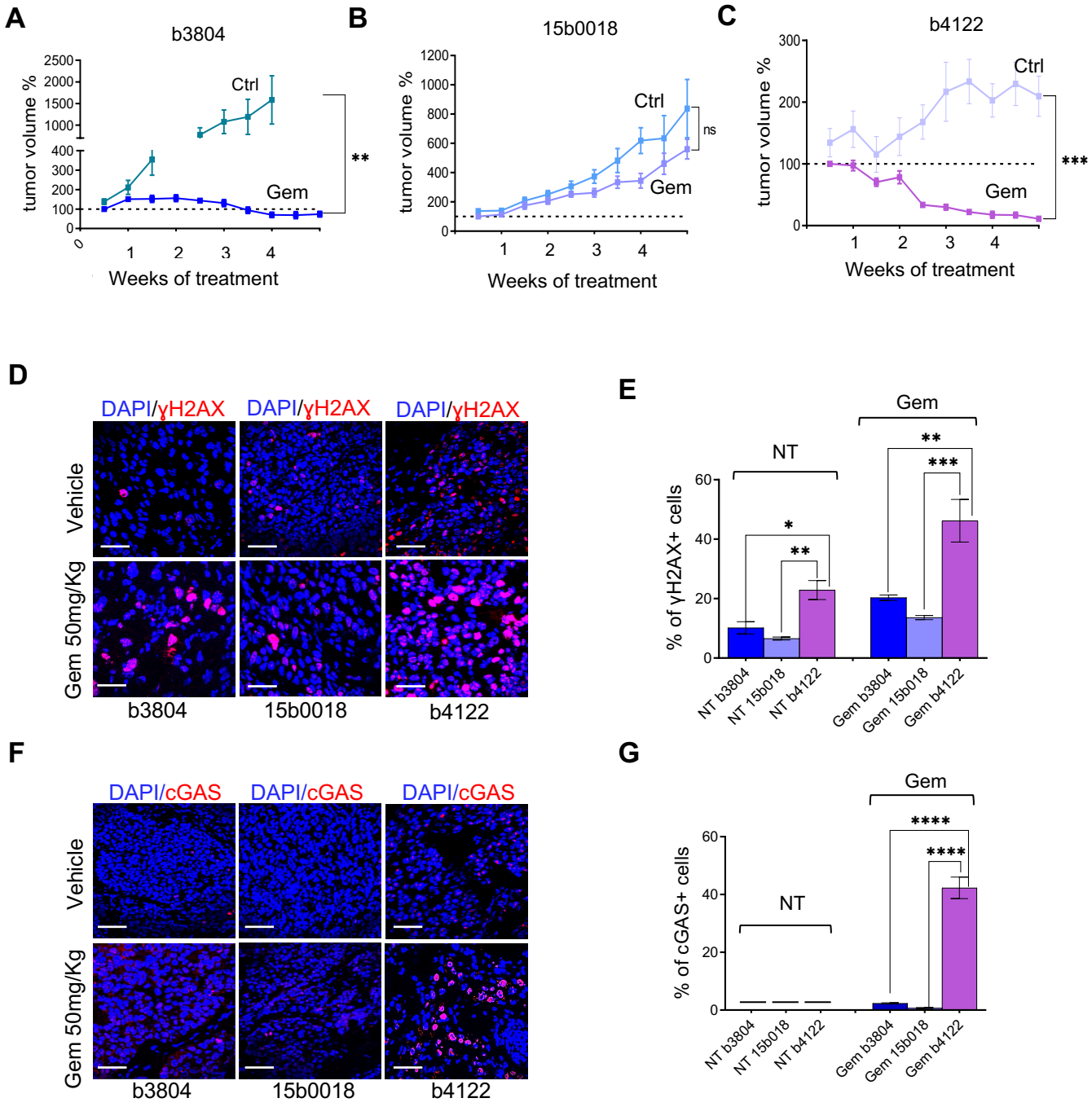
A
b3804
tumor volume %
Ctrl
Gem
**
Weeks of treatment
B
15b0018
tumor volume %
Ctrl
Gem
ns
Weeks of treatment
C
b4122
tumor volume %
Ctrl
Gem
***
Weeks of treatment
D
DAPI/γH2AX
DAPI/γH2AX
DAPI/γH2AX
Vehicle
Gem 50mg/Kg
b3804
15b0018
b4122
E
Gem
NT
**
***
*
**
% of γH2AX+ cells
NT b3804
NT 15b018
NT b4122
Gem b3804
Gem 15b018
Gem b4122
F
DAPI/cGAS
DAPI/cGAS
DAPI/cGAS
Vehicle
Gem 50mg/Kg
b3804
15b0018
b4122
G
Gem
NT
****
****
% of cGAS+ cells
NT b3804
NT 15b018
NT b4122
Gem b3804
Gem 15b018
Gem b4122

Figure 7

Figure 7: TNBC PDX showing good response to gemcitabine exhibit increased γH2AX and cGAS staining. A, B, C, D: growth curves of PDX b15b0018 , b3804, b1995 and b4122; black lines mock, red lines gemcitabine-treated. About 50mm3 of tumors were grafted subcutaneously to 8 mice in each experimental arm and treatment started when tumor volume had reached 150mm3 on average. Two injections/week of 50mg/kg gemcitabine were administered by IP injection for 4 weeks. Mice in the control arms were injected with the vehicule. **E, F:** γH2AX immunostaining and quantification of positive cells**. G, H:** cGAS immunostaining and quantification of positive cells. Statistical significance was assessed using the non-parametric Student t-test. P-values were considered as significant when *, ≤ 0.05 and highly significant when **, ≤ 0.01; ***, ≤ 0.005 ; ****, ≤ 0.001. Scale bars : 50µm